Tunability of CuOx properties by gas flow rate control in the reactive DC magnetron sputtering

C. VITELARU[*], I. PANA, A. E. KISS, N. C. ZOITA, A. VLADESCU, M. BRAIC
National Institute of Research and Development for Optoelectronics - INOE 2000, 409 Atomistilor St., 077125, Magurele, Romania

The reactive magnetron sputtering process of Cu target in Ar/O_2 atmosphere is described in a wide interval of reactive gas flow rate fractions, ranging from 0 to 70 %. The experiments took place in the constant pressure mode, at 0.67 Pa constant pressure. The gas flow ratios were calculated to take into account the differences in the pumping speeds for different gases. This approach makes possible the distinct evaluation of the oxygen gas losses due to the reactive processes inside the plasma chamber. The pressure and voltage variations, along with optical emission intensity variations of the selected lines during the hysteresis experiments are used to describe and identify the process windows. Considering a selected number of critical points on the process window, thin films of CuO_x were deposited and characterized. The transition from Cu_2O to CuO structure was assessed by XRD analysis, and confirmed by the optical properties of the films. The films with higher Cu content were identified as Cu_2O, with direct optical band gap values in the range of 2.53 to 2.41 eV, whereas lower Cu content films were identified as CuO with indirect band gap values in the range of 1.13 to 1.09 eV. Moreover, a reliable concordance between the variations of process parameters and thin film properties was obtained.

1. Introduction

Reactive magnetron sputtering is one of the most used technological processes for obtaining compound thin films [1-4]. The description of the process is usually performed by using the so-called hysteresis effect, characterizing the non-linear behaviour of the system at the variation of reactive gas content into the gas mixture [5, 6]. The hysteresis behaviour is frequently looked at as a non-desired feature of the process, leading to unstable functioning and consequent difficulties in obtaining the requested stoichiometry and properties of the film. Therefore, considerable effort is made either to diminish this effect [6, 7], or to stabilize the process via an active control loop [8]. Nevertheless, working inside the transition region can be of practical interest, the deposition of new sub-stoichiometric compounds becoming possible [1]. However, active systems or robust experimental procedures are in high demand for stabilizing the deposition process.

Although some of the main aspects concerning the experimental procedure used for acquiring and interpreting the hysteresis loop are commonly reported in the literature, there is no universal definition of all parameters to be controlled or monitored. As previously reported, for acquiring the hysteresis loop one needs to register the data after a certain "steady state" is reached [6, 9]. Another point of consensus throughout the literature is related to the pumping speed, considered as key parameter, which can be used to tune the width of the hysteresis loop in an effective way [1, 5, 10], up to the point where it is completely removed, if the pumping speed exceeds a

critical value [10]. Considering the investigation of the hysteresis occurring due to the variation of reactive gas content, the gas flow rate, pumping speed and pressure control represent several approaches reported in the literature. These approaches are different in terms of parameters to be controlled versus parameters that are allowed to freely adapt to the process conditions and act as indicators of the reactive processes. The constant pressure mode implies the use of an active control loop either for the pumping speed [11] or for the Ar flow rate [12], such as the total pressure inside the chamber remains constant throughout the whole interval. Another common approach is to fix both the pumping section and the inert gas flow rate [6], so that the addition of reactive gas leads to an increase of both reactive gas partial pressure and total pressure. One alternative, providing a mixture between constant pumping speed and constant pressure modes is to adjust both the reactive gas and the Ar flow rates, keeping the sum of the two flow rates constant [13]. The fine variation of Ar flow rate was proposed as an alternative to achieve better stability in the transition region [1]. In this work we report on this approach, making one step further, by taking into account the different pumping speeds of the involved gases, and correcting the Ar flow rate so that the total pressure measured without plasma is constant.

The proposed experimental procedure is assessed in an experiment related to the sputtering of Cu target under Ar/O_2 reactive atmosphere, aiming to obtain tuneable composition and properties of the resulting copper oxide film. In the past several decades, the copper oxide films have attracted much interest due to their composition containing earth abundant materials, non-toxicity and low

fabrication costs [14, 15]. Copper oxide (CuO_x) is a *p*-type semiconductor which may form three distinct phases Cu_2O (cuprite or cuprous oxide), CuO (cupric oxide) and Cu_4O_3 (paramelaconite) [16].

Up to now, CuO_x, especially Cu_2O - which is a direct bandgap semiconductor, have been extensively used in energy conversion and optoelectronic devices, such as solar cells [17, 18] and light emitting diodes [19-21], mostly due to its large band gap values and high absorption coefficient in the visible region [22]. Several authors reported both direct [23, 24] and indirect [25] allowed band gap energy values for these copper oxide materials. The reported band gap energy values of Cu_2O and CuO thin films are ranging from 1.9 to 2.6 eV and from 1.2 to 2.05 eV, respectively [22, 26-31].

CuO_x is also considered to be a promising multifunctional material, to be used for a wide range of applications including optics, sensing, tribology, electrochemistry, electrochromics, photocatalysis or high temperature superconductivity area [14, 32].

Depending on the oxidation state and on the production technique used, the copper oxides exhibit different properties. There are different studies focused mainly on reactive gas flow rate variation and power input reporting on the influence of the external control parameters on the physical and chemical properties of copper oxides [26, 33, 34].

In this study we will focus on the tunability of the properties of coper oxide obtained by magnetron sputtering, in relation to the key process parameters of reactive sputtering process, by proper identification and description of reliable process windows.

2. Experimental setup

The experiments were performed using a custom-made deposition unit equipped with a 2" magnetron, schematically presented in Fig. 1. The pumping system included a Maglev magnetically levitated turbomolecular pump (300 l/s), backed up by a preliminary vacuum pump. The base pressure of 1.4×10^{-4} Pa was reached before each experiment, both for the deposition process and plasma emission measurements.
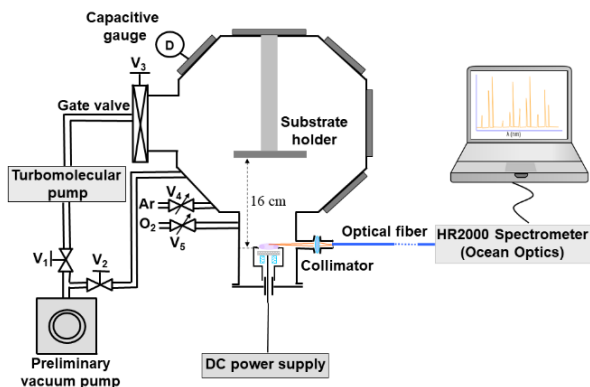

Fig. 1. Experimental setup

The light emitted from the intense plasma region in front of the target was collected by using a collimator mounted between the optical quartz window and the optical fibre, which was connected to the HR2000 spectrometer (Ocean Optics-USA). The plasma emission spectra were recorded in the 180 to 900 nm wavelength interval.

CuO_x coatings were deposited at room temperature on 1 mm thick (10 x 15 mm^2) glass substrates (Heinz-Herenz, Hamburg, Germany) and on Si (100) coupons, placed at 16 cm from target surface, on grounded substrate holder with no additional heating. Reactive magnetron sputtering of a Cu target (99.99 % purity, 50 mm diameter, 5 mm thick, from Kurt Lesker) was employed in a mixture of argon and oxygen reactive atmosphere for different O_2 mass flow ratios, i.e., $Fr = Q_{O_2}/Q_{total}$. The argon and oxygen (both 99.999 % purity) were introduced into the main chamber via two mass flow controllers. The oxygen flow ratio F_R was varied from 0 % to 60 %, while maintaining the pumping section and turbopump rotation speed constant. The gate valve position was fixed such as a total gas pressure of 0.67 Pa was obtained for 5 sccm Ar flow rate, measured without any plasma, condition called "plasma off" hereafter. The total gas pressure during the reactive magnetron sputtering experiments was monitored using absolute pressure MKS-Baratron Capacitance Manometer. The Cu cathode was powered by a DC power supply by controlling the discharge current and monitoring the voltage as a process parameter that adapts to the process conditions, through the plasma impedance.

The optical properties of the CuO_x thin films were investigated by UV-Vis-NIR spectroscopy, the transmission (T) and reflectivity (R) measurements being assessed using a Jasco 670 spectrophotometer with an attached ARSN-733 unit with a 60 mm integrating sphere. The spectra were recorded with a 400 nm/min scan speed in the 365 – 1240 nm range. The transmission measurements were made at normal incidence, while the absolute reflectance measurements were performed with the normal to sample's surface oriented at 15^0 relative to both incident beam and detector.

Phase composition of thin films on Si substrates was analysed by grazing-incidence X-ray diffraction (GIXRD) using a Rigaku's SmartLab diffractometer equipped with 9kW Cu rotating anode. The primary beam was parallelized by a Gober mirror, passed a 2-bounce Ge(220) monochromator to select the $CuK_{\alpha 1}$ radiation, and then collimated by 0.05 mm × 5 mm primary slits before hitting the sample under an incident angle of $\omega = 1°$. The 0.05 mm height value of the width limiting slit was chosen to assure a small enough footprint width of the incident beam on the sample surface, in order to do not alter the instrument resolution (do not supplementary broaden the Bragg peaks). An HyPIX-3000 detector was used for detection of the diffracted X-ray photons. The detector worked in 1D mode, the active strip covering about 5.8° on 2Θ direction. The GIXRD diffractograms were recorded on 30° to 80° 2Θ range with a step size of 0.02° and an acquisition speed of 1°/min.

The thickness of test films used for estimation of the deposition rate in different conditions was measured from a step height in a masked area on the substrate with a surface profiler (Dektak 150 Veeco).

3. Results

3.1. Reactive sputtering process characterization

The reactive sputtering is a complex process, involving inter-related surface and volume phenomena, leading to non-linear behaviours. On one side, these characteristics can lead to process instabilities, but can also be beneficial when trying to tune the properties of the thin films through the variation of key process parameters. The approach we followed for this purpose was to separate the effects of each parameter, in order to pinpoint its effects on process stability and tunability.

The main tools we used for the characterization of the reactive process are:

i) *Optical Emission Spectroscopy (OES)* – providing local information from inside the high-density plasma region, embedding cumulative effect of particle densities (atoms and charged particles),

ii) *current/voltage characteristics* - offering overall information on total plasma impedance, including surface and volume effects,

iii) *absolute pressure measurements* - providing information on the total gas pressure inside the process chamber. Depending on measuring conditions, these data can provide an indirect measure of the reactive gas dynamics.

3.1.1. Evaluation and adjustment of gas feed and pumping for reactive magnetron process

Due to the gettering effects of metal atoms that act as an additional selective pump for reactive gas, there is a difference between the pressure measured with plasma and without plasma, as previously reported [1, 10]. Therefore, by applying the total pressure control mode, the actual background pressure is not constant, the constant pressure value being the resultant of reactive gas flow rate change, chemisorption and consequent pumping to the walls, and pumping section modifications determined by the active control loop. It is also known that the pumping speed depends on the specific gas to be pumped [35], this characteristic being usually overlooked when dealing with processes involving multiple gases, such as the reactive sputtering. As this characteristic is specific to each pumping system, it is necessary to individually evaluate the effect of pumping speed variation for each system, running in conditions close to the ones used for the desired process. In our case, the starting set-point for the measurements corresponded to 0.67 Pa total pressure and constant Ar flow rate (5 sccm). Both the pumping section and turbopump rotation speed corresponding to these conditions were kept constant throughout all the experiments presented in this section.

In case of "plasma off" conditions, the pressure variation registered while increasing the gas flow rate in the 0.5 to 5 sccm interval is represented in Fig. 2a, both for Ar and O_2 gas feeding, the continuous lines representing a linear fit of the registered data. Although the pressure difference between the two types of gases might seem small, this will give rise to changes of the total pressure when replacing the same amount of Ar with O_2 in. Indeed, the pressure variation when increasing O_2 flow rate, while reducing the Ar one, in order to maintain the same total gas flow rate, is represented in Fig. 2b, showing a decrease from 0.67 Pa to 0.59 Pa when fully replacing Ar with an equivalent flow rate of O_2 (5 sccm). The observed decrease, directly related with the pumping speed differences for the two gases, can be misleading when trying to describe the reactive sputtering mode. The virtual "pumping to the walls" as described by Berg's model [3] cannot be separated in this case, being partially masked by this pressure variation.
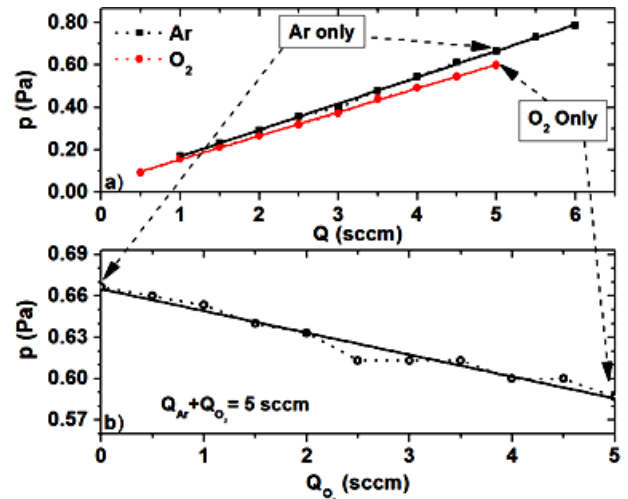

Fig. 2. The measured pressure variation vs. gas flow rate, for different gas feeding conditions: single gas Ar or O_2 a), Ar + O_2 mixture at 5 sccm constant total flow b). The turbopump rotation speed and valve opening were fixed to ensure a constant pressure (0.67 Pa) for 5 sccm Ar flow, without plasma

The next step was to evaluate, for this particular system, the Ar flow rate correction needed to obtain the same total pressure (0.67 Pa) for O_2 flow rate increase from 0 to 4.5 sccm. Fig. 3a shows the variation of Ar flow rate when increasing the O_2 flow rate, in two cases: 0.67 Pa constant total pressure and 5 sccm constant total flow rate. Comparing the red and dotted black curves in Fig. 3a, it can be seen that the Ar flow rate is higher in the first case along the entire interval. When keeping the pressure constant, the total flow rate goes as high as 6.6 sccm for 4.5 sccm of O_2, i.e 1.1 sccm of Ar instead of 0.5 sccm at constant total flow rate.

The continuous red line in Fig. 3a represents a linear fit of the registered gas flow rates, and was used in the following to compute the needed Ar flow rate for each value of the O_2 flow rate in the variation interval. Although both gas flow rates represent the control parameters, the dependencies that will be presented in the

following refer to the reactive gas flow fraction, i.e $Fr = Q_{O_2}/Q_{total}$. Therefore, the Fr dependency on the reactive gas flow rate is also represented in Fig. 3b, for both control modes. As expected, Fr value is slightly lower for the same oxygen flow rate when the total pressure is kept constant, because the total flow rate is increased by Ar flow rate correction.
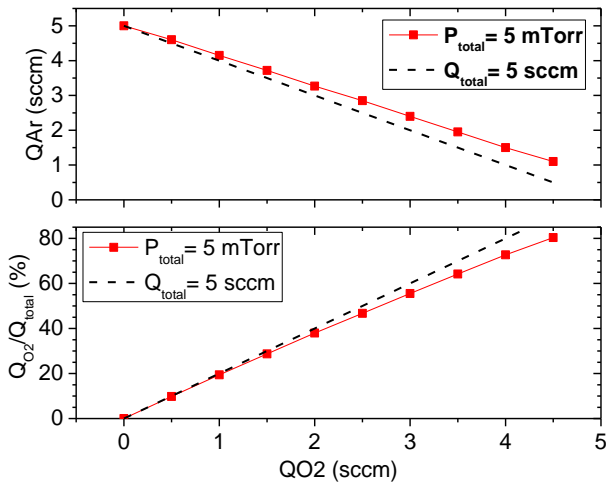

Fig. 3. Ar flow rate a) and reactive gas fraction Fr b) variations, versus the O_2 flow rate, corresponding to either a constant total pressure (0.67 Pa) or to a constant total flow rate (5 sccm). The turbopump rotation speed and valve opening was fixed to ensure a constant pressure (0.67 Pa) for 5 sccm Ar flow rate

By applying the correction of Ar gas flow rate, the background pressure remains constant whereas the total gas pressure measured during the reactive process becomes a valuable parameter in the description of hysteresis effect, making possible the understanding of gas consumption processes (especially to the walls), as discussed in the following.

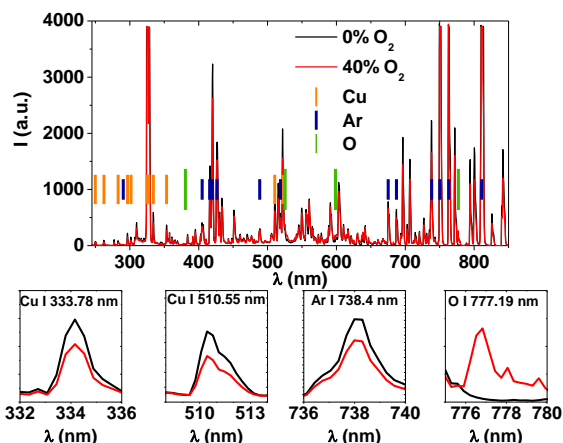### 3.1.2. Main species identification through optical emission spectroscopy

Fig. 4. Typical emission spectra and emission lines identified for two discharges (I_{DC}=150 mA, P_{total} = 0.67 Pa)

Optical emission spectroscopy was used as a non-invasive tool to obtain volume related information needed for the identification of the reactive process parameter windows. The first step for performing OES is the identification of characteristic emission lines for each of the species involved in the reactive process, i.e Ar, Cu and O. Fig. 4 presents typical emission spectra, acquired in Ar atmosphere and Ar/O₂ gas mixture, respectively. The discharge current and the total gas pressure were kept constant, 150 mA and 0.67 Pa respectively. Based on known transitions listed in NIST database [36], and emission lines identified in similar conditions and reported in the literature [37], the representative lines were identified, being marked (Fig. 4) by vertical coloured bars. A few emission lines were selected among these, and the corresponding emission spectra intervals are represented in the insets of Fig. 4. The selected emission lines are used in the following for the characterization of the reactive process and the hysteresis behaviour.

3.1.3. Process intervals identification

The data extracted from the hysteresis behaviour examination produce significant knowledge needed to describe the reactive sputtering processes [2, 5, 38]. We used the gas flow rate values and corresponding gas flow fractions as previously deduced, corresponding to a constant total pressure p=0.67 Pa under "no plasma" conditions (Fig. 3b). The current intensity was kept constant at 150 mA. Fig. 5a presents the total pressure and cathode voltage variations at the reactive gas flow fraction increase and decrease, while in Fig. 5b is presented the corresponding variation of the selected emission lines intensities. All the parameters were registered in quasi-stationary conditions, with 3 to 5 minutes delay from the moment when the gas flow rate change occurs.
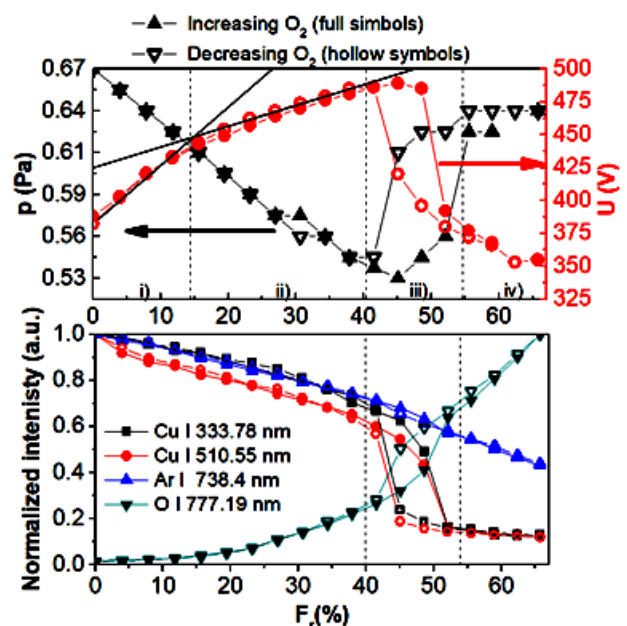

Fig. 5. Hysterezis behaviour for target cathode voltage and total pressure a); selected emission lines b), I_{DC}=150 mA, P_{total}=0.67 Pa for "plasma off" conditions

When following the variation interval, between 0 and 75 % of O_2 flow rate, one can identify at least 4 distinct intervals of variation, marked in Fig. 5 from i) to iv). These intervals correspond to different states of the system (target and walls surfaces, volume, etc), corresponding to potentially different properties of the deposited thin films, as described in the following.

i) Fr=0─15 %, the quasi metallic mode; it begins the formation of the compound on the target surface, which increases slowly as the reactive gas flow rate increases. A quasi linear voltage increase is observed, related both with oxide formation on the target and the decrease of total pressure and Ar partial pressure. As shown by Depla et al. [39], the discharge voltage behaviour is strongly related to the ion induced secondary electron emission (ISEE) of the target surface. In the case of Cu the ISEE of the oxide is smaller than the one of the metallic target, leading to higher voltages at same discharge current. A linear decrease of the total pressure is observed in this interval, mainly due to the oxide formation on the surfaces and corresponding Oxygen consumption, acting like a selective pumping term [5]. The Cu and Ar emission lines slowly decrease, following the changes of both target surface and gas composition, while the O emission line remains constant around the noise level, as the oxygen density is still too small to be detected

ii) Fr=15 %─40 %, the previously described tendencies are continuing, apart from two sizeable changes: the slope variation of the target voltage and the slow increase of oxygen emission line intensity. The change of the slope at 15% of O_2 flow rate marks the passage to a regime where the target contamination becomes important, and the target surface is gradually covered by compound, as the O_2 flow rate increases. The target contamination is fully reversible in this interval, as all the registered parameters follow the same path at the increase or decrease the O_2 flow rate. Indeed, this represents a productive interval from the deposition point of view, potentially enabling the tunability of film properties, as the process is stable without enforcing any other supplementary precautions.

iii) Fr=40 %─55 % marks the so-called "hysteresis interval", where significant differences are measured for the parameters measured at the increase or the decrease of the reactive gas flow rate. Indeed, when increasing the oxygen flow rate an abrupt voltage decrease is observed, corresponding to the passage to a fully oxidized target surface. The voltage drop is coupled with a pressure increase towards values close to "no plasma" conditions, and a corresponding increase of the oxygen emission line. This indicates a dramatic decrease of the oxygen pumping to the walls, closely related with the reduction of Cu sputtering, as shown by the decrease of Cu emission lines in this interval. The reversal of voltage variation slope goes against the decrease of secondary electron emission

coefficient for oxide compared to metal target. This shows that other mechanisms are involved in reducing the overall resistance of the discharge, such as presence of considerable amount of negative oxygen ions, changes in the electron distribution function, and corresponding changes in the ionization efficiency [40]. As for the comparison between the increasing vs decreasing part of the curves, the higher total pressures and oxygen emission intensity on the decreasing part are clear indicators of the total poisoning of the walls.

iv) Fr>55 % corresponds to a fully poisoned regime, where all surfaces are fully covered with the oxide layer. The voltage and total pressure values are identical when increasing and decreasing the oxygen flow rate respectively, corresponding to a fully oxidized target and almost zero pumping term to the walls. Note that a small decrease of pressure in Ar/O_2 mixture is registered, showing that part of the oxygen content is still trapped into the oxide deposited on the walls and target. The oxygen density in the plasma volume steadily increases in this interval, as it can be seen by the quasi-linear increase of the oxygen emission line. Note that the approximation of emission line intensity variation with density variation is reasonable in this interval, since both voltage and current intensity are constant, giving same excitation conditions for the emitting atoms.

After analysing the hysteresis behaviour and corroborating the data with the electrical characteristics, gas pressure and optical emission intensities, it was concluded that the relevant process intervals for obtaining tuneable copper oxides correspond to regions ii), and iii), with Fr values situated between 12 and 56 %.

3.2. Thin film deposition and characterization

Thin copper oxide films deposition using different oxygen contents was performed in the same experimental setup as the one used for the process characterization. All samples were deposited using the same current intensity, 150 mA and a total gas pressure of 0.67 Pa (measured without plasma, with variable total gas flow rate as indicated in Fig. 3). Prior to deposition, the gas flow rates were gradually modified, by increasing the O_2 flow rate and decreasing the Ar flow rate, until the desired deposition conditions were attained.

In this way, before each deposition, the reactive flow fraction increased gradually from zero to the desired value. Such as the entire "rising" branch of the hysteresis was run-through, simulating the experimental conditions during the hysteresis measurement procedure, for getting similar conditions both for process description and thin film deposition.

Table 1. Deposition parameters and thicknesses of the samples obtained by DC magnetron sputtering

Sample	Q_{O2} (sccm)	F_r (%)	Q_{Ar} (sccm)	Thickness (nm)	Deposition rate (nm/min)
S1	0.60	12	4.50	154	6.2
S2	1.00	19	4.15	321	12.8
S3	1.50	29	3.71	282	11.3
S4	2.25	42	3.10	255	12.7
S5	3.00	56	2.40	174	2.9

3.2.1. Structural analysis

Fig. 6 shows the XRD diffractograms of the investigated coatings. The diffraction peaks were identified according to the CuO (ICDD no.04-015-5869), Cu_2O (ICDD no.04-003-6433) and Cu (ICDD no.04-0836). As expected, the coatings structure, as visualised by the diffraction patterns, strongly depend on the oxygen flow rate fraction, such as they can be classified according to the process intervals ii) and iii), as identified previously in Fig. 5.
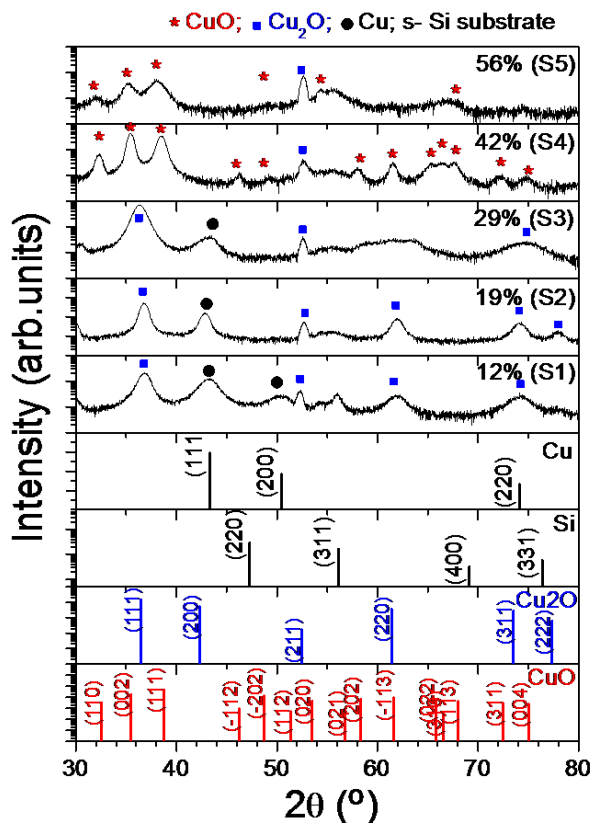

Fig. 6. XRD diffractograms of coper oxide thin films obtained at different oxygen flow rate fractions (marked in the figure). I_{DC}=150 mA, P=0.67 Pa (without plasma)

At low oxygen flow rate, F_r =12 %, the oxygen content of the S1 sample is low, leading to the formation of a mixture of cubic phases of Cu and Cu_2O, with different oxygen content. The diffraction pattern of the S1 sample (Fig. 6) contains features corresponding to $Cu_2O(111)$ and $Cu_2O(220)$ identified at 36.76° and 61.86°, respectively, Cu(220) at 50.28°, and mixed contribution of $Cu_2O(200)$ + Cu(111) and $Cu_2O(311)$ + Cu(220) at about

43.1° and 74.40°, respectively.. The measured 2θ Bragg lines positions corresponding to the Cu and Cu_2O phases lead to a value of the lattice parameter of 3.625 Å and 4.232 Å, respectively, The lattice parameter of Cu phase is slightly larger than that of pure Cu (3.615 Å, ICCD 004-0836), while the lattice parameter of Cu_2O phase is slightly smaller than that of stoichiometric Cu_2O (4.250 Å, ICDD 04-003-6433). These results suggest that the Cu_2O phase is sub-stoichiometric, oxygen deficient, while the Cu phase is not pure metallic, but has some oxygen content. The crystallite size of the cuprite phase deduced from the FWHM of the $Cu_2O(111)$ maximum following the Debye- Scherrer's formula is about 7.2 nm.

Contrary, further increasing the F_r to 29 % (Sample S3, Fig. 6), the crystallite size decreases to 6.9 nm, as well as the lattice parameter to 4.230 nm. The diffraction pattern contains a part from specific cuprite maxima, which are visibly enlarged in comparison with those of the S2 sample, some features developed in the 57° - 68° 2θ range. These features could arise due to the inset of a CuO phase formation. In such a case the Cu_2O phase could be de-oxygenated as a fraction of oxygen would be used for the formation of the CuO phase, which is, however, richer in oxygen than the Cu_2O phase. In consequence, we assume that the structure of the S3 sample consists of polycrystalline Cu_2O grains and an almost amorphous matrix of CuO phase.

Further increasing the oxygen flow rate to F_r = 42 % (S4 sample), only the CuO phase is formed. The main features identified in the diffraction pattern of the S4 sample at about 32.25°, 35.41°, and 38.45° can be attributed to the (110), (002), and (111) planes, respectively, of the body-centred monoclinic structure of CuO (ICDD 04-015-5869). The lattice parameters a=4.670 Å, b=3.467 Å, and c= 5.130 Å deduced from the positions of the above mentioned Bragg maxima, are in very good agreement with those of the reference data ICDD 04-015-5869 (a=4.684 Å, b=3.445 Å, c=5.131 Å), suggesting that the film composition is closed to the stoichiometry of CuO. In consequence, it is expected that the sample S5, grown at higher oxygen flow rate, F_r = 56 %, contains oxygen in excess. The features identified in the S4 sample diffraction pattern are present in that of S5 sample too, but obviously enlarged. That could be due to interstitially incorporation of the excess oxygen. This hypothesis is confirmed by the enlargement of the S5 film lattice cell, whose lattice parameters, a=4.71 Å, b=3.49 Å, c=5.15 Å, are considerably larger than those from the reference data, ICDD 04-015-5869. That result was to be expected, as long as the S5 sample was grown in fully poisoned target

condition (Fig. 5). The average grain size values deduced from the FWHM of the CuO(110), CuO(002) and CuO(111) decreases from 11.8 nm, 12.95 nm, and 10.42 nm to 5.7 nm, 7.4 nm, and 5.4 nm respectively, as the oxygen flow rate fraction is increased from 42 % (S4 sample) to 56 % (S5 sample).

Our results are in good agreement with those reported by other researchers, indicating that phase formation in CuO_x coatings can be controlled by adjusting only the plasma conditions during the deposition, through the oxygen flow rate [26, 41-43]. Additional control over the phase formation can be obtained by combining gas flow rate variation with changes of substrate conditions, through biasing or by post-deposition annealing of CuO_x films [27].

3.2.2. Optical and electronic band properties

The absorption coefficient of the CuO_x films deposited on glass substrates was deduced over the 365 nm – 1240 nm spectral range from the transmission (T) and reflectance (R) spectra using the formula:

$$\alpha = (1/d)\ln((1-R)/T), \tag{1}$$

where d is the thickness of the film measured by surface profilometry (Table 1). The CuO_x films are highly absorbing, with absorption coefficient values of the order of 2×10^5 at photon energies above the absorption threshold. The band gap values were extracted according to Tauc's algorithm [44] by extrapolation of the linear regions of $f(hv) = (\alpha hv)^m$ plots to the photon energy axis [26], where $m = 2$ or $\frac{1}{2}$ for direct or indirect allowed transitions, respectively. Fig.7a) presents the Tauc' plots corresponding to S2 – S5 samples. Note that S1 sample was not analysed because of its reduced transparency, due to high Cu content. In order to choose which type of transition corresponds to each type of film, all the curves were represented for both m=2 and ½ values. The best fit for a linear region was identified on the $f(hv) = (\alpha hv)^2$ plots, corresponding to CuO_x films with lower oxygen content (S2 and S3 samples), indicating a direct bandgap material, whilst a good linearity was revealed for $f(\alpha h) = (\alpha hv)^{1/2}$ plots corresponding to CuO_x films, with higher oxygen content (S4 and S5 samples), indicating indirect transitions. These results are in agreement with the XRD investigations (Fig.6) which show a phase transition from cubic-structured Cu_2O phases (S2 and S3 samples) to monoclinic structured CuO phases (S4 and S5 samples). At the same time, our results are in agreement with the literature data which generally reported Cu_2O as direct and CuO as indirect semiconductors, respectively [26-29]. Some discrepancies can be found when classifying the type of bandgap for CuO_x, being assigned to the variations in growth conditions and methods, leading to different crystalline qualities, indicating the formation of multi-phase CuO_x films [26].
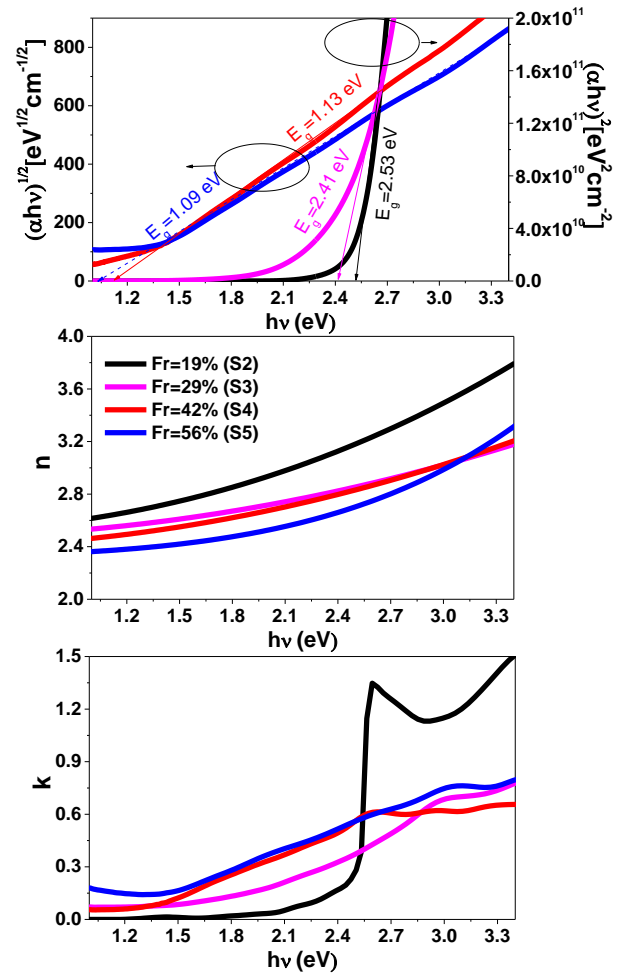

Fig. 7. Tauc plot (a), refractive indices (b) and extinction coefficients (c) of S2-S5 CuO_x layers obtained at different gas flow ratios (I_{DC}=150 mA, p~0.67 Pa)

When the oxygen flow rate fraction is increased from F_r=19 % (S2 sample) to F_r=29 % (S3 sample), the direct optical band gap shows a decrease from 2.53 eV to 2.41 eV, values which are both in good agreement with the 2.33 ÷ 2.6 eV reported values by Balamurugan et al. and Pierson et al. [27, 45]. Furthermore, by increasing the oxygen flow rate fraction to $F_r = 42$ % (S4 sample) and further to $F_r = 56$ % (S5 sample), the Cu_2O-CuO phase transition occurs and the indirect band gap values are decreasing to 1.13 and 1.09 eV respectively. For the oxygen-rich films, the band gap values are also similar to those reported by Ooi et al. [26], who found that CuO films have an indirect band gap of approximatively 1.2 eV. The slightly smaller bandgap values of S4 and S5 samples could be due to the different structural properties of our films [26].

It is known that films of copper oxides strongly absorb light below the 600 nm wavelength (i.e photon energies > 2.06 eV) [45] and their optical behaviour in the visible spectral range can be better described in terms of optical parameters such as refractive index (n) and extinction coefficient (k). In this work, the n and k coefficients were deduced over the 1 - 3.4 eV photon energy range from T and R spectra using the OptiChar software [46, 47]. Fig.7b and 7c show the energy

dependence of n and k coefficients corresponding to S2 – S5 samples. On the visible spectral range, the refractive index of the CuO_x films was decreasing with increasing oxygen content. The sample S2 (F_r=19 %) is the only one which presented a higher refractive index and a sharp increase of extinction coefficient above 2.4 eV (Fig. 7). This result can be related to XRD diffractogram, which showed that only this sample exhibits only Cu_2O peaks. For sample S3 (F_r =29 %) presents a mixture of Cu_2O and CuO, as revealed by XRD results, and also confirmed by the optical properties. As the phase transition from Cu_2O to CuO happen when the oxygen F_r is increased from 29 % to 42 %, the n values corresponding to S3 and S4 samples have quite close values, despite the different oxygen content. Further increase of oxygen F_r to 56 % leads to a small decrease of refractive index, with negligible changes of the extinction coefficient. From the XRD and optical results, one can conclude that at F_r=42 % it was enough oxygen available for CuO formation, and a further increase (F_r=56 %) produced just a small decrease of the band gap from 1.13 eV to 1.09 eV. Figs. 7a and c indicate a good correlation between $(\alpha h v)^{1/m}$ and $k(hv)$ plots, confirming that the type of transition (direct or indirect) have been correctly assigned to the S2 ─ S5 samples.

3.3. Discussions

Conclusively, for linking the process intervals portrayed in Fig. 5 and the properties of thin films, Fig. 8 presents some key parameters which describe the reactive process along with the main parameters defining the thin films properties.
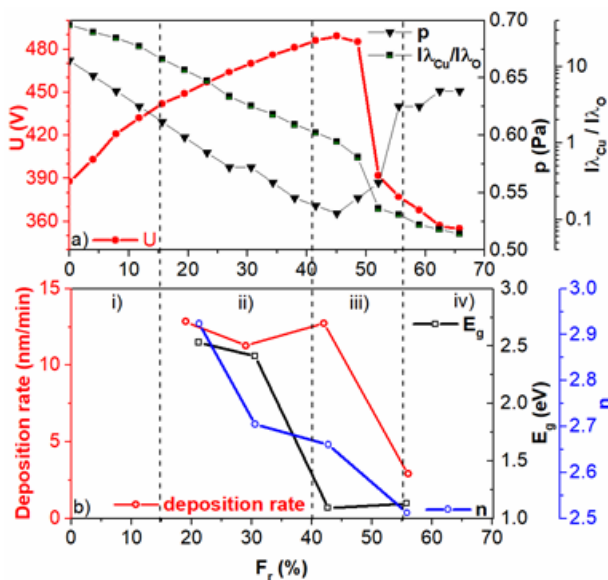

Fig. 8. a Target voltage, total pressure and line intensity variation (Cu I 333.78 nm and O I 777.194 nm) when increasing the F_r from 0 to 65%; b) Optical band gap values, the refractive index at 633 nm and the deposition rate variation for the investigated samples (S1-S4). Discharge current was kept constant at 150 mA

Fig. 8 shows the best fitted plasma parameters which describe the process intervals: target voltage, total gas pressure and the ratio of the Cu I 333 nm and O I 777 line intensities. A good correlation between the identified process windows and film properties can be seen, with Cu rich Cu_2O thin films in the interval ii) and O rich CuO films in the interval iii). Although the samples deposited in interval iii) have very close band gap values, they are distinguished by a high difference between their deposition rates. This is directly related with the positioning of process parameters close to the metal to compound transition, with F_r=42 % situated towards the metal mode and F_r=56 % towards the compound mode, as previously reported in the literature [34].

4. Conclusions

An experimental procedure for the description and control of the reactive sputtering process and corresponding film properties was developed. The approach consisted in the variation of gas flow ratios, corrected for the differences in pumping efficiency of Ar and O_2. By doing so, a constant total pressure under no-plasma conditions was maintained for all experimental conditions. This allowed the use of total pressure variation as a reliable indicator of the gas consumption by the reactive processes inside the discharge volume. Both Ar and O_2 flow rates were adjusted such as to get a variable total gas flow, permitting to obtain the desired oxygen flow rate ratio variation. The procedure was implemented for the DC magnetron reactive sputter deposition of CuO_x in Ar/O_2 atmosphere. The reactive process was described by using a combination of OES, discharge electrical parameters measurement, and total gas pressure variation. The exact identification of transition points and intervals describing the reactive process allowed us to define the most suitable process conditions, permitting to tune the films properties, such as to obtain either direct or indirect bang-gap Cu oxide films. The obtained thin films have variable oxygen content, being identified as Cu_2O for conditions corresponding close to the metallic mode, and CuO for conditions corresponding to the edges of the hysteresis loop. The tunability of the oxide properties was therefore achieved by using the knowledge gained from process description, such as the obtained film properties were closely linked to the peculiarities of the identified process windows. The implementation of such a procedure enables to better control the deposition process and to achieve films with tunable properties.

References

[1] J. Musil, P. Baroch, J. Vlcek, K. H. Nam, J. G. Han, Thin Solid Films **475**(1-2), 208 (2005).

[2] S. M. Diederik Depla, S. Mahieu, Reactive Sputter Deposition, Springer-Verlag Berlin Heidelberg, 301, 2008.

[3] M. A. M. Patwary, K. Saito, Q. Guo, T. Tanaka, Thin Solid Films **675**, 59 (2019).

[4] A. Dulmaa, H. Vrielinck, S. Khelifi, D. Depla, Sputter Appl. Surf. Sci. **492**, 711 (2019).

[5] S. Berg, T. Nyberg, Thin Solid Films **476**(2), 215 (2005).

[6] E. Sarhammar, K. Strijckmans, T. Nyberg, S. Van Steenberge, S. Berg, D. Depla, Surf. Coat. Tech. **232**, 357 (2013).

[7] M. Aiempanakit, T. Kubart, P. Larsson, K. Sarakinos, J. Jensen, U. Helmersson, Thin Solid Films **519**(22), 7779 (2011).

[8] M. Audronis, V. Bellido-Gonzalez, B. Daniel, Surf. Coat. Tech. **204**(14), 2159 (2010).

[9] H. Barankova, S. Berg, P. Carlsson, C. Nender, Thin Solid Films **260**(2), 181 (1995).

[10] S. Kadlec, J. Musil, H. Vyskocil, J. Phys. D. Appl. Phys. **19**(9), L187 (1986).

[11] N. Nayan, M. Z. Sandan, L. J. Wei, M. K. Ahmad, J. Lias, A. Y. M. Shakaff, A. Zakaria, A. F. M. Zain, 11th Asian Conference on Chemical Sensors **20**, 124 (2016).

[12] S. Ohno, Y. Kawaguchi, A. Miyamura, Y. Sato, P. K. Song, M. Yoshikawa, P. Frach, Y. Shigesato, Sci. Technol. Adv. Mat. **7**(1), 56 (2006).

[13] I. Pana, C. Vitelaru, N. C. Zoita, M. Braic, Plasma Process. Polym. **13**(2), 208 (2016).

[14] A. S. Zoolfakar, R. A. Rani, A. J. Morfa, A. P. O'Mullane, K. Kalantar-Zadeh, J. Mater. Chem. C **2**(27), 5247 (2014).

[15] D. Prasanth, K. P. Sibin, H. C. Barshilia, Thin Solid Films **673**, 78 (2019).

[16] M. Heinemann, B. Eifert, C. Heiliger, Phys. Rev. B **87**(11), 5 (2013).

[17] L. C. Chen, Mat. Sci. Semicon. Proc. **16**(5), 1172 (2013).

[18] T. K. S. Wong, S. Zhuk, S. Masudy-Panah, G. K. Dalapati, Materials **9**(4), 21 (2016).

[19] S. Kim, K. Hong, K. Kim, I. Lee, J. L. Lee, J. Mater. Chem. **22**(5), 2039 (2012).

[20] T. Ding, X. Y. Yang, L.Y. Bai, Y. B. Zhao, K. E. Fong, N. Wang, H. V. Demir, X. W. Sun, Org. Electron. **26**, 245 (2015).

[21] G. Filipic, U. Cvelbar, Nanotechnology **23**(19), 16 (2012).

[22] J. F. Su, Q. Niu, R. R. Sun, X. Y. An, Y. S. Zhang, J. Optoelectron. Adv. M. **20**(7-8), 441 (2018).

[23] C. L. A. Ricardo, M. D'Incau, M. Leoni, C. Malerba, A. Mittiga, P. Scardi, Thin Solid Films **520**(1), 280 (2011).

[24] H. Akbari, Y. Azizian-Kalandaragh, J. Optoelectron. Adv. M. **20**(3-4), 175 (2018).

[25] D. X. Wu, Q. M. Zhang, M. Tao, Phys. Rev. B **73**(23), 6 (2006).

[26] P. K. Ooi, S. S. Ng, M. J. Abdullah, H. Abu Hassan, Z. Hassan, Mater. Chem. Phys. **140**(1), 243 (2013).

[27] J. F. Pierson, A. Thobor-Keck, A. Billard, Appl. Surf. Sci. **210**(3-4), 359 (2003).

[28] H. C. Lu, C. L. Chu, C. Y. Lai, Y. H. Wang, Thin Solid Films **517**(15), 4408 (2009).

[29] A. S. Reddy, S. Uthanna, P. S. Reddy, Appl. Surf. Sci. **253**(12), 5287 (2007).

[30] A. S. Reddy, H. H. Park, V. S. Reddy, K. V. S. Reddy, N. S. Sarma, S. Kaleemulla, S. Uthanna, P. S. Reddy, Mater. Chem. Phys. **110**(2-3), 397 (2008).

[31] A. A. Ogwu, E. Bouquerel, O. Ademosu, S. Moh, E. Crossan, F. Placido, Acta Mater. **53**(19), 5151 (2005).

[32] H. M. Yang, J. Ouyang, A. D. Tang, Y. Xiao, X. W. Li, X. D. Dong, Y. M. Yu, Mater. Res. Bull. **41**(7), 1310 (2006).

[33] K. Lim, J. Park, D. G. Kim, J. K. Kim, J. W. Kang, Y. C. Kang, Appl. Surf. Sci. **258**(22), 9054 (2012).

[34] J. F. Pierson, D. Wiederkehr, A. Billard, Thin Solid Films **478**(1-2), 196 (2005).

[35] W. Becker, Vacuum, **16**(11), 625 (1966).

[36] A. Kramida, Y. Ralchenko, J. Reader, NIST ASD Team: Nist Atomic Spectra Database -version 5.0, (2013).

[37] L. Kevin, N. Nafarizal, S. Mohd Zainizan, M. Abd Kadir, A. Mohd Khairul, M. S. Ali Yeon, Z. Ammar, A. S. Fathinul Syahir, M. Z. Ahmad Faizal, Adv. Mater. Res.-Switz. **832**, 243 (2014).

[38] S. Berg, E. Sarhammar, T. Nyberg, Thin Solid Films **565**, 186 (2014).

[39] D. Depla, S. Heirwegh, S. Mahieu, J. Haemers, R. De Gryse, J. Appl. Phys. **101**(1), 9 (2007).

[40] A. Rizk, S. B. Youssef, S. K. Habib, Vacuum **38**(2), 93 (1988).

[41] A. K. Kunti, S. K. Sharma, M. Guptab, Ecs J. Solid State Sc. **5**(10), P627 (2016).

[42] T. Serin, S. Gurakar, H. Ot, A. Yildiz, N. Serin, Appl. Surf. Sci. **352**, 155 (2015).

[43] Y. Wang, J. Ghanbaja, F. Soldera, P. Boulet, D. Horwat, F. Mucklich, J. F. Pierson, Acta Mater. **76**, 207 (2014).

[44] J. Tauc, Amorphous and liquid semiconductors, Plenum Publishing Corporation, 159, 1974.

[45] B. Balamurugan, B. R. Mehta, Thin Solid Films **396**(1-2), 90 (2001).

[46] I. Pana, C. Vitelaru, A. Kiss, N. C. Zoita, M. Dinu, M. Braic, Mater. Design **130**, 275 (2017).

[47] A. V. Tikhonravov, M. K. Trubetskov, OptiLayer Software v. 11.65e. http://optilayer.com/, (2016).

*Corresponding author: catalin.vitelaru@inoe.ro